The effect of the beta phase on the micromechanical response of dual-phase titanium alloys

Patrick J. Ashton [a], Tea-Sung Jun [b], Zhen Zhang [c], T. Benjamin Britton [c], Annette .M. Harte [d], Sean B. Leen [a], Fionn P.E. Dunne [c]

[a] Mechanical Engineering, National University of Ireland, Galway, Ireland

[b] Department of Mechanical Engineering, Incheon National University, Incheon, Republic of Korea

[c] Department of Materials, Imperial College, London, UK

[d] Civil Engineering, National University of Ireland, Galway, Ireland

Abstract

This paper investigates the role of beta phase on the micro-mechanical behaviour of dual-phase titanium alloys, with particular emphasis on the phenomenon of cold dwell fatigue, which occurs in such alloys under room temperature conditions. A strain gradient crystal plasticity model is developed and calibrated against micro-pillar compression test data for a dual-phase alpha-beta specimen. The effects of key microstructural variables, such as relative beta lath orientation, on the micromechanical response of idealised alpha-beta colony microstructures are shown to be consistent with previously-published test data. A polycrystal study on the effects of the calibrated alpha-beta crystal plasticity model on the local micromechanical variables controlling cold dwell fatigue is presented. The presence of the alpha-beta phase is predicted to increase dwell fatigue resistance compared to a pure alpha-phase microstructure.

1. Introduction

Titanium alloys are commonly used in aerospace applications due to their superior properties, including high strength to weight ratios and toughness. Extensive research has been carried out on the microstructure sensitivity of these materials, such as the assessment of crystallographic orientation [1], grain size [2] and morphology [3] in order to understand failure mechanisms, and hence, better predict service life of components. This paper investigates the effect of α–β colonies on micromechanical deformation response and failure parameters in Ti-6242, a two phase material comprised of a primary α–phase and α-β colony regions.

Crystal plasticity (CP) modelling has been previously implemented to assess the microstructure sensitivity of dual-phase titanium alloys. However, the α–β phase has previously been modelled as a single, homogenised, microstructural unit [4]–[7] where the β -phase is not explicitly modelled. In this paper, the β-phase is explicitly included in computational models, and the heterogeneous material model is calibrated against micro-pillar tests, specifically designed to elucidate the effects of the β-laths.

The small lengths associated with α-β colonies suggest that length-scale effects may be important. Length-scale effects can arise from the presence of geometrically necessary dislocations (GNDs) in the crystal lattice, which are required to accommodate plastic strain-gradients [8], [9]. GNDs act as pinning points for mobile dislocations, causing slip system hardening. Much work on length-scale effects in polycrystals considers grain size as a key length-scale. Hall [10] and Petch [11] observed an increase in material strength as grain size is reduced, commonly known as the Hall-Petch effect. Fleck et al. [12] performed torsional tests on copper wires and found that a pronounced size effect occurs where effective lengths are 10 μm or lower. Dunne et al. [1] implemented a strain-gradient crystal plasticity

modelling approach to study the effect of length-scales on stress and plastic strain across grain interfaces. A considerable increase in stress and decrease in accumulated plastic strain at grain boundaries was observed when the average grain size was reduced from 20 μm to 2 μm. Dunne et al. [13] also successfully predicted the experimentally determined distribution of GND density in near-α Ti and single crystal nickel alloy with this strain-gradient crystal plasticity finite element model. Sweeney et al. [14] implemented a similar modelling methodology to predict the effect of measured grain size on stabilized cyclic stress-strain hysteresis loops for CoCr alloy. A key length-scale for α–β colonies in Ti alloys is the α–phase ligament width (spacing between β laths), which is typically only several microns [15], [16].

The role of α–β colonies in cold dwell is investigated in this paper. Failure in dwell fatigue is understood to occur from the nucleation of quasi-cleavage micro-cracks of length approximately equal to grain size, known as facets. This process, known as 'faceting', is a key factor in the service life of several aerospace components, such as compressor rotor spools [17]. A dwell fatigue cycle includes a load holding period, which leads to a significant drop in component life in many titanium alloys compared to standard fatigue loading [18]. For example, Kassner et al. [19] observed that the number of cycles to failure for dwell fatigue tests were up to an order of magnitude lower than for equivalent standard low cycle tests. This is attributed to the ability of these materials to undergo creep at low temperatures. It has been previously shown that strain accumulation due to cold creep during the load-holding dwell period leads to load shedding from a favourably oriented grain to an adjacent unfavourably oriented grain with respect to the loading direction [18], [20], [21]. This creep-induced load-shedding process is considered critical for facet nucleation.

In this paper, a crystal plasticity computational study is performed to assess the global and local behaviour of α–β colonies in Ti-6242. A crystal plasticity finite element model is developed with calibration and validation against measured micropillar tests on α–β Ti-6242. The role of α–phase ligament width, length-scale effects, and α–phase crystallographic orientation are assessed using representative models of α–β colonies. β laths are explicitly represented in these models based on previous experimental observations [15]. This work implements a physically-based approach for calculation of GND density, based on plastic strain-gradients, without the need to specify additional length terms. Hence, the length-scale is derived purely from the geometry of the model. Later in the paper, the role of α–β colonies is assessed in the context of cold dwell. α–β colony location and orientation with respect to a rogue grain combination is analysed. This work is relevant to microstructure design of dual phase titanium alloys for resistance to crack nucleation in cold dwell fatigue.

2. Crystal Plasticity Model

It is assumed that planar glide is the primary deformation mechanism in this material at temperatures and strain rate regimes relevant to cold dwell fatigue. Deformation by twinning is not considered in this work as Ti-6242 contains a high aluminium content, which has been shown to significantly reduce twinning deformation in titanium alloys [22]. The rate-sensitive, length-scale dependent crystal plasticity model of Dunne et al. [1] is implemented in this computational study to describe crystallographic slip. An overview of the constitutive model is given here. Readers are referred to Ref [1] for a more detailed description of the original computational implementation. The existing material model formulation has been modified to calculate GND density following the approach of Cheng and Ghosh [23].

The following slip rule [1] which relates slip rate to shear stress is based on the strain rate equation by Gibbs [24] where gliding dislocations are controlled by pinning at obstacles, such

as precipitates or sessile dislocations. The slip rate $\dot{\gamma}^{\alpha}$ is related to shear stress τ^{α} on a slip system α by

$$\dot{\gamma}^{\alpha} = \rho_{SSD}^{m} \nu b^{\alpha 2} \exp\left(\frac{\Delta H}{-kT}\right) sinh\left(\frac{(\tau^{\alpha} - {\tau_c}^{\alpha})\gamma_0 \Delta V^{\alpha}}{kT}\right) \quad (1)$$

where ${\rho_{SSD}}^{m}$ is the density of statistically stored mobile dislocations, ν is the frequency of attempts (successful or otherwise) by dislocations to jump the energy barrier, b^{α} is Burger's vector, ΔH is Helmoltz free energy, k is the Boltzman constant, T is temperature, ${\tau_c}^{\alpha}$ is the critical resolved shear stress on a particular slip system and $\gamma_0$is a reference strain. The activation volume ΔV on a slip system α is defined by

$$\Delta V^{\alpha} = l b^{\alpha 2} \quad (2)$$

where l is the pinning distance between dislocations, which is related to the density of immobile SSDs, ${\rho_{SSD}}^{s}$ as follows:

$$l = \frac{1}{\sqrt{\rho_{SSD}^{s}}} \quad (3)$$

Taylor hardening [25] is chosen to describe the evolution of critical resolved shear stress, which is dependent on dislocation density:

$${\tau_c}^{\alpha} = {\tau_{c0}}^{\alpha} + MGb^{\alpha}\sqrt{\rho_{GND} + \rho_{SSD}^{s}} \quad (4)$$

where ${\tau_{c0}}^{\alpha}$ is the initial critical resolved shear stress for a slip system α, G is material shear modulus, M is the Taylor factor and ρ_{GND} is the GND density.

The GND density on a slip system is calculated by relating closure failure due to the presence of dislocations on a plane per unit area, as described by Nye [8], to the plastic deformation gradient:

$$\sum_{\alpha=1}^{nslip} \boldsymbol{b}^{\alpha} \otimes \boldsymbol{\rho}^{\alpha} \; = \; curl(\boldsymbol{F}^{\mathrm{p}}) \tag{5}$$

where $\boldsymbol{F}^{\mathrm{p}}$ is the plastic deformation tensor. Dislocations can be of edge type, screw type or mixed character [26]. Dislocation density on a slip system can therefore be decomposed into three components $\boldsymbol{\rho}_{\mathrm{s}}^{\alpha}$, $\boldsymbol{\rho}_{\mathrm{et}}^{\alpha}$ and $\boldsymbol{\rho}_{\mathrm{en}}^{\alpha}$ to give:

$$\sum_{\alpha=1}^{nslip} (\boldsymbol{\rho}_{\mathrm{s}}^{\alpha} \boldsymbol{b}^{\alpha} \otimes \boldsymbol{s}^{\alpha} + \; \boldsymbol{\rho}_{\mathrm{et}}^{\alpha} \boldsymbol{b}^{\alpha} \otimes \boldsymbol{n}^{\alpha} + \boldsymbol{\rho}_{\mathrm{en}}^{\alpha} \boldsymbol{b}^{\alpha} \otimes \boldsymbol{t}^{\alpha}) = curl(\boldsymbol{F}^{\mathrm{p}}) \tag{6}$$

where $\boldsymbol{s}^{\alpha}$ is the slip direction, $\boldsymbol{n}^{\alpha}$ is slip normal, and $\boldsymbol{t}^{\alpha} = \boldsymbol{s}^{\alpha} \times \boldsymbol{n}^{\alpha}$. A matrix of dyadic products $\boldsymbol{A}$ can be constructed to give

$$\boldsymbol{A}\boldsymbol{\rho} = curl(\boldsymbol{F}^{\mathrm{p}}). \tag{7}$$

A total of 12 potentially active slip systems are considered to contribute to $\boldsymbol{\rho}$ [23], for which, a unique solution does not exist, as there are fewer equations than unknowns. The least squares minimization procedure, as described by Arsenlis and Parks [27], is implemented here to calculate $\boldsymbol{\rho}$. A singular value decomposition technique is employed to determine the pseudo inverse of $\boldsymbol{A}$. The GND density used in Eq. (4) is the sum of the squares of dislocation density on all 12 potentially active slip systems. Knowledge of the plastic deformation gradient at each integration point within an element is required to determine $curl(\boldsymbol{F}^{\mathrm{p}})$. For this reason, the above constitutive model is implemented as a User Element Subroutine (UEL) in the finite element code ABAQUS. The methodology for calculating spatial gradients of $\boldsymbol{F}^{\mathrm{p}}$ is described by Kiwanuka [28].

3. Material

The primary α–phase is a hexagonal close packed (HCP) lattice system with 24 slip systems, as shown in Fig 1. The α–β regions contain a HCP α–phase and body centre cubic (BCC) β laths. The crystal plasticity model described here is implemented for the HCP α-phase of this material. Previous experimental work regarding the behaviour of individual α–β colonies in dual-phase titanium alloys has shown that a key consideration when analysing these colonies is the existence of a Burgers Orientation Relationship (BOR) [29], [30] between the HCP α–phase and BCC β-phase, where the closest packed planes and directions are shared between the two phases. However, the β phase is considered to be isotropic elastic in this work as the observations of Jun et al [15] show significantly lower slip levels in the β phase of this material under pillar compression tests. Further, since it is the α–β interfaces and their influence on plastic strain gradients and GND density which are key aspects of this study, considering the β phase to be elastic provides a worst-case scenario, or conservative approach, in consideration of the effects in cold dwell fatigue.

The elastic β-phase properties used here are those identified by Kim and Rokhlin [31]. The anisotropic elastic properties for the α–phase are taken from the experimental tests of Hasija et al. [20] on Ti-6Al. The α–phase activation energy ΔH for Ti-6242 has been calibrated in previous work by Zhang et al. [32] using single phase micro-pillar compression test data. This property reflects the rate sensitivity of the material, which is important for the cold dwell problem addressed in this work. Experimental results from Jun et al. [15] are implemented to calibrate critical resolved shear stress τ_{c0} and Taylor hardening constant M for the CPFE model, as discussed later. The critical resolved shear stresses for prismatic and basal slip systems are assumed to be equal, based on the negligible difference in strengths between these slip systems, as observed by Hasija et al. [20]. The <c+a> pyramidal type slip systems

are assigned slip strengths approximately three times higher than <a> type systems, in agreement with experimental results of Gong and Wilkinson [33]. Only <a> type slip systems are considered here for the calculation of GND density as Britton et al. [34] observed significantly lower densities on <*c*+*a*> type slip systems in Ti-6Al-4V. A list of material parameters used in the slip rule is given in Table 1. Tables 2 and 3 present the elastic constants for each phase of the material.

Fig. 2 shows a measured phase map for a typical α–β colony in dual-phase titanium alloys [35]. In this work, finite element models are generated using an idealised α–β lath geometry as shown in Fig. 2b. This assumption allows for the development of structured element meshes and mesh densities giving practical computational run-times.

4. CPFE Model Calibration

Jun. et al [15] performed compression tests on α–β micro-pillar specimens of Ti-6242. These experimental results have been adopted here to calibrate and validate the CPFE model. A finite element representative model of a α–β micro-pillar is developed to calibrate the critical resolved shear stress and slip system hardening by comparing global force-displacement with corresponding experimental measurements. The pillar specimen geometry is shown in Fig. 3. The substrate is modelled as an isotropic elastic material, based on previous simulations of pure α–phase micro-pillars [32]. Length-scale effects are included in this analysis as the presence of the β-phase is expected to result in high gradients of plastic strain near phase interfaces, and thus, significant hardening due to the presence of GNDs. The bottom face of the substrate is fixed in all directions and a compressive displacement is applied to the top face of the pillar to replicate the experimental test. A mesh sensitivity has been carried out to ensure the results presented here are mesh independent.

Fig. 4 shows a comparison of the calibrated CPFE predicted force-displacement response, both with and without length-scale effects, and the measured experimental response. The inclusion of length-scale effects causes a harder predicted response due to the evolution of GND density. A critical resolved shear stress τ_{c0} of 240 MPa and Taylor factor M of 0.3 are chosen for the material model as they show excellent agreement with the experimentally observed force-displacement response. These parameters are used for the subsequent analysis in this paper.

5. α–β Colony Study

Jun et al. [15] observed that the stress-strain behaviour of nine micropillar specimens varied significantly with respect to β–phase morphology. This experimental work suggests the need to isolate key microstructural features to gain a better understanding of the behaviour of α–β colonies. Computational modelling is attractive in this context, due to the difficulty associated with the experimental fabrication of test specimens for analysis of specific features in complicated microstructures.

This section presents a systematic study on the effects of α–phase ligament width and relative α–phase crystallographic orientation in order to further understand the deformation mechanisms in α–β colonies. Finite element unit cell models of α–β colonies are generated as discussed above. The β lath width is fixed at 0.5 μm in all analyses based on the observations of Jun et al. [15] for the as-received material. Three different α–phase ligament widths, 1 μm, 2 μm and 5 μm, are considered, as shown in Fig. 5.

The boundary conditions used in these compression simulations are shown in Fig. 6. All vertical faces of the model are unconstrained, to simulate the behaviour of a single colony

under compression. A displacement is applied to the top face of the model, corresponding to 2.5% engineering strain at a strain rate of 1×10^{-3} s^{-1}.

Fig. 7 shows the predicted effect of α–phase ligament width on the compressive stress-strain response, both with and without length-scale effects. The α–phase in this analysis is oriented so the primary slip direction is nearly-perpendicular to β laths as shown in Fig. 5c. As α-phase ligament width is reduced, a harder response is observed. This effect is attributed to the increasing number of β laths in the model microstructure, and thus, a greater volume fraction of β-phase, which is assumed to be elastic. Similarly, length-scale effects increase as ligament width decreases. The number of phase boundaries increases as ligament width decreases, resulting in a larger proportion of the model with high strain-gradients, and therefore, increased GND hardening, as shown by the contour plots of GND density in Fig. 8.

In order to investigate the effect of α–phase crystallographic orientation with respect to β laths, three different α-phase orientations, as shown in Fig. 9, are analysed as follows: (a) primary slip direction near-perpendicular to β laths, (b) primary slip direction near-parallel to β laths, and (c) crystal c-axis parallel to loading direction. For cases (a) and (b) primary slip planes are shown with a red hatching in Fig. 9. Where the crystal c-axis is parallel to the loading direction, as in case (c), there are no easily activated slip systems. The unit cell model in Fig. 5b is implemented here in each case, applying the same boundary conditions as in Fig. 6. Fig. 10 shows the compressive stress-strain response for cases (a) and (b). Case (a) displays the hardest global stress-strain response. Considering first the mechanistic basis of crystal slip in α-β colonies, crystallographic slip is anticipated to be inhibited by the β laths, which act as barriers for mobile dislocations on the primary adjacent slip system. Within the crystal plasticity framework, slip transfer by dislocation transit is not explicitly captured, but is so indirectly through strain compatibility requirements. The primary slip direction in case

(b) is near-parallel to β laths, and thus, there is no barrier for mobile dislocations, leading to a significantly softer response. This is shown schematically in Fig. 11. Length-scale effects are more significant in case (a) due to a higher GND density at phase α–β interfaces. It should be noted that the stress-strain response for cases (a) and (b) are identical when β laths are excluded from the analysis, as the Schmid factors on the primary slip systems are equal.

Fig. 12 shows a comparison of the unit cell compressive stress-strain response for all three α–phase orientation cases, for which all <*a*>- and <*c* +*a*>- type slip systems are included and may potentially be activated. In case (c), where the crystal c-axis is oriented parallel to the loading direction, <*a*> type slip systems are difficult to activate, resulting in a significantly harder response. <*c*+*a*> type pyramidal slip systems become active at a larger macroscopic strain than the other cases.

This effect of relative α-phase orientation presented here was also observed in previous experimental work of [16], [36]. Suri et al. [36] investigated the stress-strain and creep behaviour of two individual colony samples. The α–phase of the samples was oriented for (a) <*a*> type slip near-parallel to the β laths and (b) <*a*> type slip oriented near-normal to the β laths. The latter, type (b), showed a higher macroscopic yield stress and increased hardening, attributed to the presence of misfit dislocations at α–β interfaces and relatively larger misalignment of primary slip systems between phases. Fig. 13 shows the stress-strain response of these two colonies adopted from Suri et al. [36]. The predicted results of Fig. 10 are clearly consistent with the measured responses of Fig. 13. For example, at a strain of 2.5%, the harder colony is shown to carry a 15% and 12% higher stress than the softer colony in Figs. 10 and 13, respectively.

6. Application to Cold Dwell

In this section, a polycrystal model of Ti-6242 is developed to assess the effect of α–β colonies on the key variables that control cold dwell fatigue. As mentioned above, the presence of a rogue grain combination is an important factor for faceting, where an unfavourably oriented 'hard' grain lies adjacent to a favourably orientated 'soft' grain with respect to crystallographic slip. A load-holding dwell period causes a redistribution of stress from soft to hard grains, due to cold creep occurring in soft grains, leading to local stress relaxation. The hard grains must therefore carry a higher stress to maintain the applied load. Dunne and Rugg [21] argue that the stress component normal to the basal plane, in the hard grain, is important in faceting; a critical stress approach was adopted to identify the facet initiation near soft-hard grain boundaries, consistent with experimental observations [37].

'Macro-zones' are also argued to be important in dwell fatigue in titanium alloys [38]. Also referred to as micro-textured regions (MTRs), these are relatively large regions (up to mm length scales) of uniform α crystallographic orientation often containing colonies of β laths. A macro-zone, which is badly oriented for slip adjacent to a softer unit well-oriented for slip, provides the potential for load shedding from soft to hard grains during dwell and for the formation of a large basal facet across the entire α unit. This has been argued to be of particular significance in dwell fatigue and in driving the 'dwell debit' [39], [40], [41].

Previous work has assessed several key factors in dwell, including microstructure morphology [3], temperature [42] and material hydrogen content [43]. In relation to the α–β phase, Venkataramani et al. [44] implemented a CPFE model, with a homogenised α–β phase [7], to study the effect of various microstructural features on creep-induced load shedding in Ti-6242. The key aspect investigated here, which has not previously been

studied, is β lath location and relative orientation with respect to a particularly unfavourable combination of α-phase grains, or rogue grain combination.

A three-dimensional polycrystal model is generated with hexagonal-shaped grains. The grain size is taken to be 10 μm, giving a fine-grained representation of this material [27]. Fig. 14 shows (a) the geometry of the model meshed with 20-noded reduced integration elements and (b) a graphical representation of the rogue grain combination considered here, where a central hard grain is oriented so that the crystal c-axis lies parallel to the loading direction and two soft grains, favourably oriented for prismatic slip. All other grains in the model are assigned random 'soft' orientations. The bottom face of the polycrystal is fixed in the y-direction, the left face is fixed in the x-direction, and the back face is fixed in the z-direction. Stress holding, which is considered to be more detrimental than strain holding in dwell fatigue [21], is analysed here, by applying a stress to the top face of the model according to the loading history in Fig. 15. A dwell period of 24 seconds is chosen to allow a significant transfer of stress from soft grains to hard grains. The applied stress of 660 MPa ensures local slip at grain boundaries and the development of GNDs but is well below conventional macroscale yield.

Four different microstructures are considered here, as shown in Fig. 16, as follows:

Base Case	α grains only.
β1	β laths located in a soft grain (forming a colony) and oriented near-parallel to α-phase primary slip direction.
β2	β laths located in a soft grain and oriented near-perpendicular to α-phase primary slip direction.

β3 β laths located in the central hard grain.

The path (labelled Path 1) shown in Fig.16a is chosen for sample distributions of stress, to demonstrate the load shedding process during the dwell period. The α-phase crystallographic orientations of each grain are identical for all microstructures considered. A mesh sensitivity has once again been carried out to ensure mesh independence of predicted responses.

7. Results and Discussion

In order to demonstrate the significance of the dwell period, the pre- and post- dwell σ_{yy} stress distributions are plotted in Fig. 17 along path 1 for the base case (pure α-phase). As seen in previous modelling work [21], the dwell period causes a significant redistribution of stress from soft grains to hard grains, leading to large post-dwell discontinuities at soft-hard grain boundaries. However, in order to assess the effect of the β-phase, it is necessary to analyse the effect on stresses over a more extensive region of the hard grain, adjacent to the grain boundary. Hence, the stresses are sampled from the entire rectangular region highlighted in Fig. 16b, to ascertain the effect of β-phase microstructure on creep dwell resistance for each of the microstructures analysed. The local maximum stress normal to the basal plane in the hard grain, has been identified as a key variable controlling facet nucleation [21]. It is therefore adopted here to quantify the effect of β laths on facet nucleation. The pre- and post-dwell value of this variable, termed σ_b^{max} here, is plotted for each microstructure in Fig. 18.

The pre-dwell σ_b^{max} is predicted to increase due to the presence of the β-phase, as shown in Fig. 18a. The β2 microstructure shows the highest σ_b^{max}, giving a 10% increase, compared to the base case. However, for all microstructures considered, the presence of β laths reduces the post-dwell σ_b^{max} in the hard grain, as shown in Fig 18b. By considering the pre- and post-

dwell histograms, it can be seen that the presence of the β-phase restricts load shedding from the soft grain to the hard grain, resulting in a lower predicted post-dwell σ_b^{max}. The most significant difference is seen in microstructure β3, where σ_b^{max} is predicted to be 12% lower than the base case. This is attributed to the lower load-carrying ability of the hard grain compared to the other microstructures due to the presence of β laths. Overall, dwell fatigue resistance is predicted to increase with the inclusion of the β-phase.

This key result is consistent with previous work regarding the effect of the β-phase on dwell fatigue life in titanium alloys. Kassner et al. [19] showed experimentally the increase in dwell fatigue resistance with the increase in volume fraction of the β-phase. Previous CPFE modelling work of Venkatramani et al. [44], albeit using an homogenised α-β phase, also showed that increased β-phase volume fraction gave reduced load shedding..

The effect of excluding length-scale effects is investigated here for the pure α-phase base case microstructure.. Fig. 19a compares post-dwell stress distributions along path AA, showing decreased grain boundary stresses with the exclusion of length-scale effects. σ_b^{max} is also predicted to decrease by 20% in the absence of GND density evolution. Higher stresses are predicted in the length-scale dependent model as a result of high GND density near grain boundaries, as shown in Fig. 19b, where the distribution of GND density is plotted along path AA. Therefore, high strain gradients exist in the polycrystal model of Ti-6242, leading to significant GND hardening, which cannot be accounted for in a length-scale independent model.

8. Conclusions

A strain-gradient, crystal plasticity model is implemented for dual-phase titanium alloy, with explicit representation of β-phase laths, and the material model is calibrated against micro-

pillar compression test data. A study of α–β colonies in Ti-6242 alloy has established increased strength as α-phase ligament width decreases, due to (i) increased β-phase volume fraction and (ii) increased GND hardening. The relative crystallographic orientation of the α–phase (with respect to β lath orientation) is determined to play a key role in the stress-strain response of α–β colonies. Colonies with an α-phase primary slip direction oriented near-perpendicular to β laths show a significantly stronger stress-strain response than colonies oriented for slip near-parallel to β laths.

Analysis of a polycrystal model of Ti-6242 has shown that explicit incorporation of α–β colonies leads to restricted inter-granular load shedding during the dwell period in a fatigue cycle, resulting in lower local stresses. Dwell fatigue resistance is therefore predicted to increase due to the presence of the β-phase, consistent with previous publications.

It is shown that the very small size-scales associated with the β laths leads to important strain gradient hardening effects, which are incorporated in the present crystal plasticity formulation via of the evolution of geometrically-necessary dislocations. It is shown that exclusion of these strain gradient effects causes a 20% under-prediction of the (critical) maximum post-dwell stress. It is therefore concluded that accurate and reliable physically-based prediction of cold dwell facet nucleation, and hence facet fatigue, requires incorporation of strain gradient effects.

9. Acknowledgments

The authors would like to acknowledge the Irish Research Council and the Engineering and Physical Science Research Council (through HexMat) for funding this work and the Irish Centre for High-End Computing (ICHEC) for the provision of computational facilities. FPED

wishes to acknowledge gratefully the provision of funding for his Royal Academy of Engineering/Rolls-Royce research chair.

10. References

[1] F. P. E. Dunne, D. Rugg, and A. Walker, "Lengthscale-dependent, elastically anisotropic, physically-based hcp crystal plasticity: Application to cold-dwell fatigue in Ti alloys," *Int. J. Plast.*, vol. 23, no. 6, pp. 1061–1083, 2007.

[2] M. A. Cuddihy, Z. Zheng, J. Gong, T. B. Britton, A. J. Wilkinson, and F. P. E. Dunne, "Grain size effects in hcp polycrystals : from GNDs to blocky alpha," In Review, 2016.

[3] F. P. E. Dunne, A. Walker, and D. Rugg, "A systematic study of hcp crystal orientation and morphology effects in polycrystal deformation and fatigue," *Proc. R. Soc. A Math. Phys. Eng. Sci.*, vol. 463, no. 2082, pp. 1467–1489, 2007.

[4] M. Zhang, J. Zhang, and D. L. McDowell, "Microstructure-based crystal plasticity modeling of cyclic deformation of Ti-6Al-4V," *Int. J. Plast.*, vol. 23, no. 8, pp. 1328–1348, 2007.

[5] O. J. McCarthy, J. P. McGarry, and S. B. Leen, "Micro-mechanical modelling of fretting fatigue crack initiation and wear in Ti-6Al-4V," *Int. J. Fatigue*, vol. 62, pp. 180–193, 2013.

[6] J. R. Mayeur and D. L. McDowell, "A three-dimensional crystal plasticity model for duplex Ti-6Al-4V," *Int. J. Plast.*, vol. 23, no. 9, pp. 1457–1485, 2007.

[7] G. Venkatramani, S. Ghosh, and M. Mills, "A size-dependent crystal plasticity finite-element model for creep and load shedding in polycrystalline titanium alloys," *Acta Mater.*, vol. 55, no. 11, pp. 3971–3986, 2007.

[8] J. F. Nye, "Some geometrical relations in dislocated crystals," *Acta Mater.*, no. 1, pp. 153–162, 1953.

[9] M. F. Ashby, “The deformation of plastically non-homogeneous materials,” *Philos. Mag.*, vol. 21, no. 170, pp. 399–424, 1970.

[10] E. O. Hall, “The Deformation and Ageing of Mild Steel: III Discussion of Results,” *Proc. Phys. Soc. Sect. B*, vol. 64, no. 9, p. 747, 1951.

[11] N. J. Petch, “The cleavage strength of polycrystals,” *J. Iron Steel Inst.*, vol. 174, pp. 25–28, 1953.

[12] N. A. Fleck, G. M. Muller, M. F. Ashby, and J. W. Hutchinson, “Strain gradient plasticity: Theory and experiment,” *Acta Metall. Mater.*, vol. 42, no. 2, pp. 475–487, 1994.

[13] F. P. E. Dunne, R. Kiwanuka, and A. J. Wilkinson, “Crystal plasticity analysis of micro-deformation, lattice rotation and geometrically necessary dislocation density,” *Proc. R. Soc. A* vol. 468, no. 2145, pp. 2509–2531, 2012.

[14] C. A. Sweeney, B. O’Brien, F. P. E. Dunne, P. E. McHugh, and S. B. Leen, “Strain-gradient modelling of grain size effects on fatigue of CoCr alloy,” *Acta Mater.*, vol. 78, pp. 341–353, Oct. 2014.

[15] T.-S. Jun, G. Sernicola, F. P. E. Dunne, and T. B. Britton, “Local deformation mechanisms of two-phase Ti alloy,” *Mater. Sci. Eng. A*, vol. 649, pp. 39–47, 2016.

[16] K. Chan, C. Wojcik, and D. Koss, “Deformation of an alloy with a lamellar microstructure: experimental behavior of individual widmanstatten colonies of an α-β titanium alloy,” *Metall. Trans. A*, vol. 12, no. November, pp. 1899–1907, 1981.

[17] S. Gosh, M. Mills, S. Rokhlin, V. Sinha, W. Soboyejo, and J. Williams, “The Evaluation of Cold Dwell Fatigue in Ti-6242,” *FAA Rep.*, no. January, 2007.

[18] M. R. Bache, “A review of dwell sensitive fatigue in titanium alloys: The role of microstructure, texture and operating conditions,” *Int. J. Fatigue*, vol. 25, no. 9–11, pp. 1079–1087, 2003.

[19] M. E. Kassner, Y. Kosaka, and J. A. Hall, “Low-cycle dwell-time fatigue in Ti-6242,” *Metall. Mater. Trans. A*, vol. 30, no. September, pp. 2383–2389, 1999.

[20] V. Hasija, S. Ghosh, M. J. Mills, and D. S. Joseph, “Deformation and creep modeling in polycrystalline Ti–6Al alloys,” *Acta Mater.*, vol. 51, no. 15, pp. 4533–4549, 2003.

[21] F. P. E. Dunne and D. Rugg, “On the mechanisms of fatigue facet nucleation in titanium alloys,” *Fatigue Fract. Eng. Mater. Struct.*, vol. 31, no. 11, pp. 949–958, 2008.

[22] J. C. Williams, R. G. Baggerly, and N. E. Paton, “Deformation behavior of HCPTi-Al alloy single crystals,” *Metall. Mater. Trans. a-Physical Metall. Mater. Sci.*, vol. 33, no. 3, pp. 837–850, 2002.

[23] J. Cheng and S. Ghosh, “A crystal plasticity FE model for deformation with twin nucleation in magnesium alloys,” *Int. J. Plast.*, vol. 67, pp. 148–170, 2015.

[24] G. B. Gibbs, “Thermodynamic analysis of dislocation glide controlled by dispersed local obstacles,” *Mater. Sci. Eng.*, vol. 4, no. 6, pp. 313–328, Sep. 1969.

[25] G. I. Taylor, “The Mechanism of Plastic Deformation of Crystals. Part I. Theoretical,” *Proc. R. Soc. A Math. Phys. Eng. Sci.*, vol. 145, pp. 3625–387, 1934.

[26] A. Ma, F. Roters, and D. Raabe, “A dislocation density based constitutive model for crystal plasticity FEM including geometrically necessary dislocations,” *Acta Mater.*, vol. 54, no. 8, pp. 2169–2179, 2006.

[27] A. Arsenlis and D. M. Parks, “Crystallographic aspects of geometrically-necessary and statistically-stored dislocation density,” *Acta Mater.*, vol. 47, no. 5, pp. 1597–1611, 1999.

[28] R. Kiwanuka, “Micro-deformation and Texture in Engineering Materials,” *PhD Thesis*, 2013.

[29] D. Bhattacharyya, G. . Viswanathan, R. Denkenberger, D. Furrer, and H. L. Fraser, “The role of crystallographic and geometrical relationships between α and β phases in an α/β titanium

alloy," *Acta Mater.*, vol. 51, no. 16, pp. 4679–4691, 2003.

[30] W. G. Burgers, "On the process of transition of the cubic-body-centered modification into the hexagonal-close-packed modification of zirconium," *Physica*, no. 7–12, pp. 561–586, 1934.

[31] J.-Y. Kim and S. I. Rokhlin, "Determination of elastic constants of generally anisotropic inclined lamellar structure using line-focus acoustic microscopy," *J. Acoust. Soc. Am.*, vol. 126, no. 6, p. 2998, 2009.

[32] Z. Zhang, T. S. Jun, T. B. Britton, and F. P. E. Dunne, "Intrinsic anisotropy of strain rate sensitivity in single crystal alpha titanium," *Acta Mater.*, vol. 118, pp. 317–330, 2016.

[33] J. Gong and A. J. Wilkinson, "Anisotropy in the plastic flow properties of single-crystal α titanium determined from micro-cantilever beams," *Acta Mater.*, vol. 57, no. 19, pp. 5693–5705, Nov. 2009.

[34] T. Ben Britton, S. Birosca, M. Preuss, and A. J. Wilkinson, "Electron backscatter diffraction study of dislocation content of a macrozone in hot-rolled Ti-6Al-4V alloy," *Scr. Mater.*, vol. 62, no. 9, pp. 639–642, 2010.

[35] T. Jun, D. E. J. Armstrong, and T. B. Britton, "A nanoindentation investigation of local strain rate sensitivity in dual-phase Ti alloys," *J. Alloys Compd.*, vol. 672, pp. 282–291, 2016.

[36] S. Suri, G. B. Viswanathan, T. Neeraj, D.-H. Hou, and M. J. Mills, "Room temperature deformation and mechanisms of slip transmission in oriented single-colony crystals of an α/β titanium alloy," *Acta Mater.*, vol. 47, no. 3, pp. 1019–1034, 1999.

[37] V. Sinha, J. E. Spowart, M. J. Mills, and J. C. Williams, "Observations on the faceted initiation site in the dwell-fatigue tested ti-6242 alloy: Crystallographic orientation and size effects," *Metall. Mater. Trans. A*, vol. 37, no. 5, pp. 1507–1518, 2006.

[38] D. Rugg, M. Dixon, and F. P. E. Dunne, "Effective structural unit size in titanium alloys," *J. Strain Anal. Eng. Des.*, vol. 42, no. 4, pp. 269–279, 2007.

[39] K. Zhang, K. V. Yang, A. Huang, X. Wu, and C. H. J. Davies, “Fatigue crack initiation in as forged Ti–6Al–4V bars with macrozones present,” *Int. J. Fatigue*, vol. 80, pp. 288–297, 2015.

[40] N. Gey, P. Bocher, E. Uta, L. Germain, and M. Humbert, “Texture and microtexture variations in a near-α titanium forged disk of bimodal microstructure,” *Acta Mater.*, vol. 60, no. 6–7, pp. 2647–2655, 2012.

[41] F. Bridier, P. Villechaise, and J. Mendez, “Slip and fatigue crack formation processes in an α/β titanium alloy in relation to crystallographic texture on different scales,” *Acta Mater.*, vol. 56, no. 15, pp. 3951–3962, 2008.

[42] Z. Zhang, M. A. Cuddihy, and F. P. E. Dunne, “On rate-dependent polycrystal deformation: the temperature sensitivity of cold dwell fatigue,” *Proc. R. Soc. A*, vol. 471, no. 2181, p. 20150214, 2015.

[43] M. Gerland, P. Lefranc, V. Doquet, and C. Sarrazin-Baudoux, “Deformation and damage mechanisms in an α/β 6242 Ti alloy in fatigue, dwell-fatigue and creep at room temperature. Influence of internal hydrogen,” *Mater. Sci. Eng. A*, vol. 507, no. 1–2, pp. 132–143, 2009.

[44] G. Venkataramani, K. Kirane, and S. Ghosh, “Microstructural parameters affecting creep induced load shedding in Ti-6242 by a size dependent crystal plasticity FE model,” *Int. J. Plast.*, vol. 24, no. 3, pp. 428–454, 2008.

Table 1. Material parameters used in CPFE modelling.

Parameter	Value
τ_0<a>	240 MPa
τ_0<c+a>	722 MPa
M	0.3
G	29022 MPa
b <a>	2.95 x 10^{-4} μm
b <c+a>	4.68 x 10^{-4} μm
k	1.38 x 10^{-23} J K^{-1}
T	293 K
ΔH	7.58 x 10^{-20} J
ν	1.00 x 10^{11} Hz
γ_0	1.32 x 10^{-4}
ρ_{SSD}^{m}	5.0 μm^{-2}
ρ_{SSD}^{s}	0.01 μm^{-2}

Table 2. Elastic constants used for the α-phase.

Parameter	Value
E_{11}	84745 MPa
E_{33}	119789 MPa
G_{12}	29022 MPa
G_{13}	40000 MPa
v_{12}	0.46
v_{13}	0.22

Table 3. Elastic constants used for the β-phase.

Parameter	Value
E	32024 MPa
v	0.46 MPa

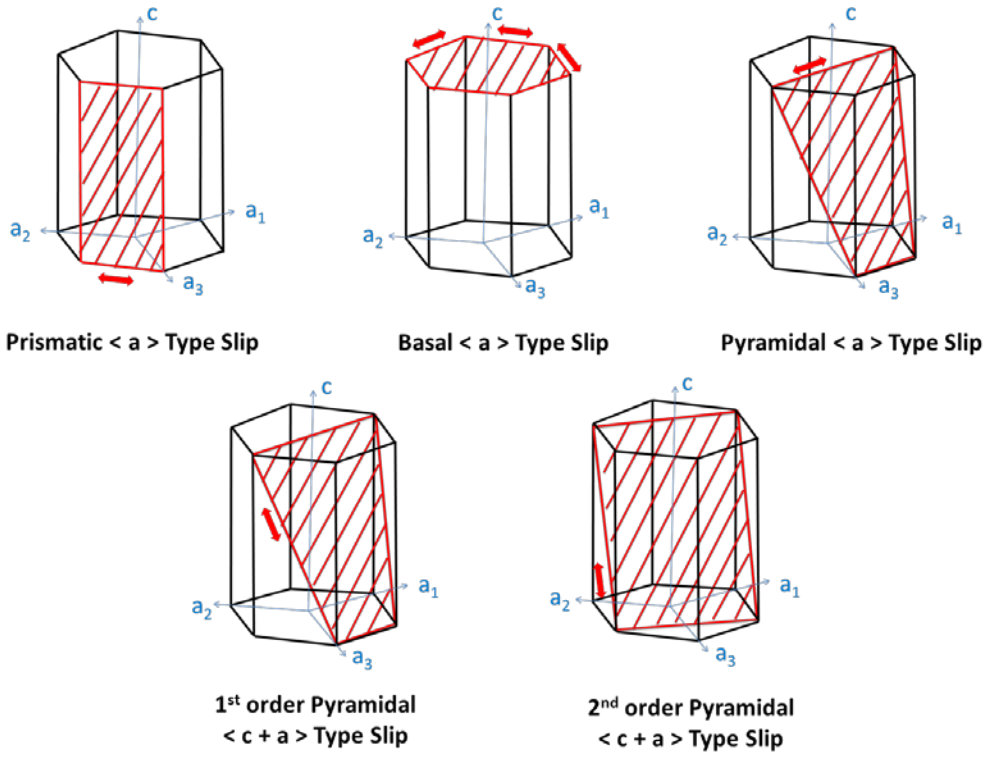

Fig. 1. Slip systems in HCP phase of titanium alloys. The red arrows indicate slip direction.

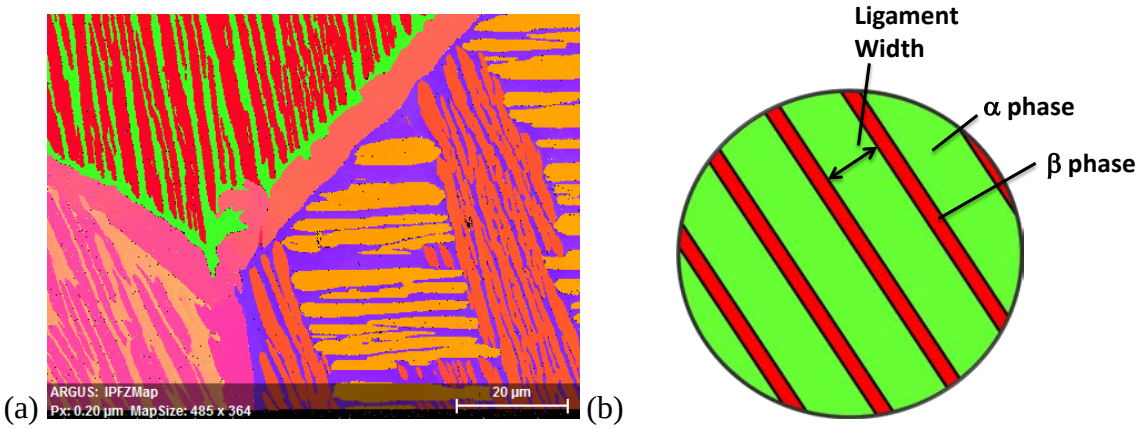

Fig 2. (a) IPF map of typical α–β colony structure in titanium alloys [35] (b) Idealised geometry for FE modelling of α–β colonies in Ti-6242

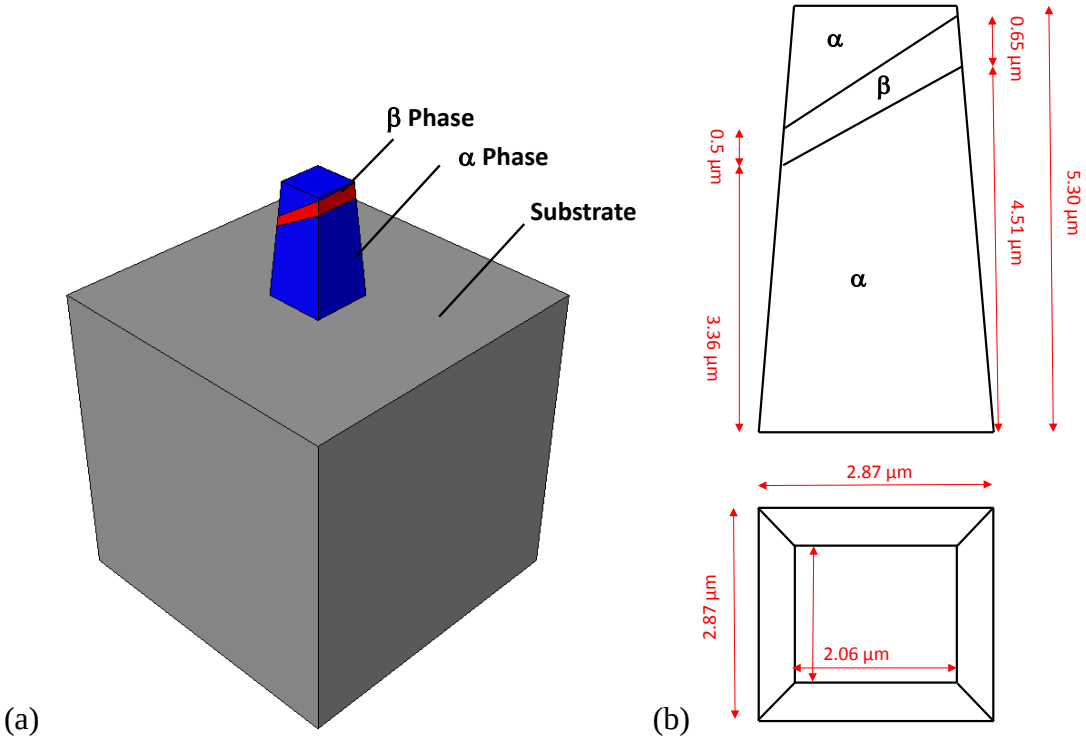

Fig. 3. (a) Finite element model of pillar specimen and (b) α–β pillar geometry.

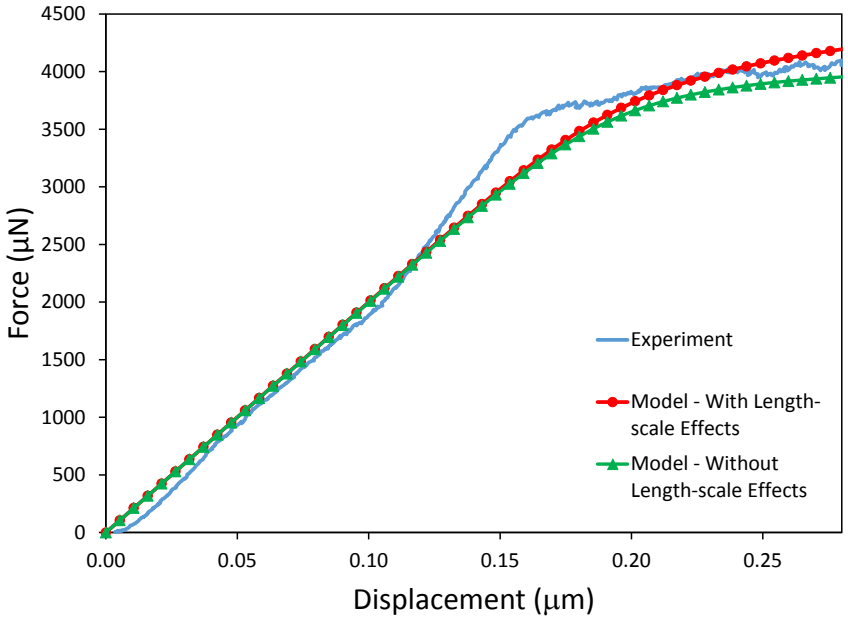

Fig. 4. Comparison of experimental and CPFE calculated (with and without length-scale effects) force-displacement response.

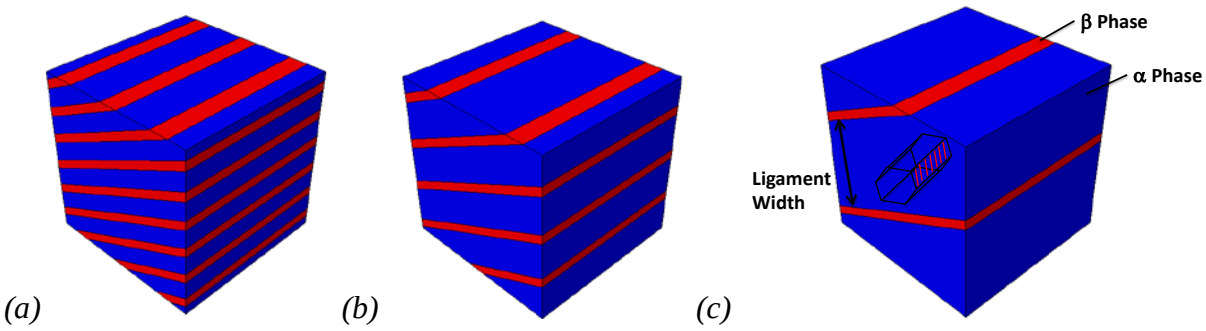

Fig.5. Idealised α–β colony model geometry for three α–phase ligament widths: (a) 1 μm (b) 2 μm (c) 5 μm showing the α–phase crystallographic orientation. α-phase primary slip systems are hatched in red

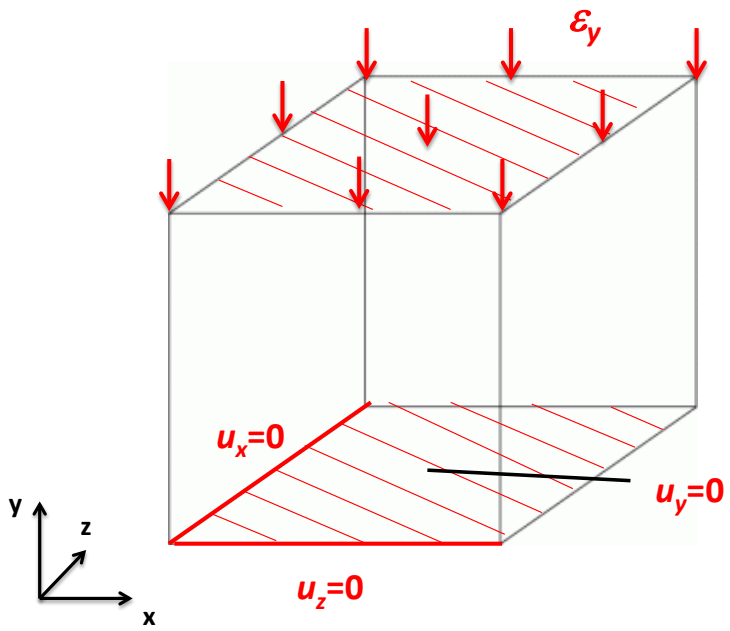

Fig.6. Boundary conditions used for compression simulations of α–β colony unit cell models.

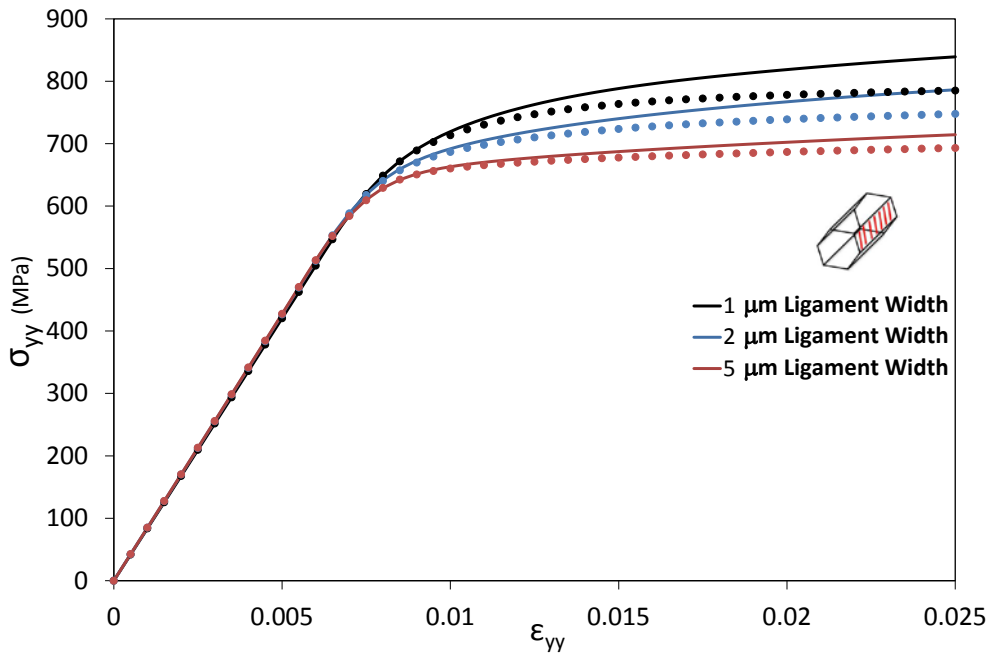

Fig.7. Global stress strain curves for α–β colony models. Dotted lines represent the exclusion of length-scale effects in analysis.

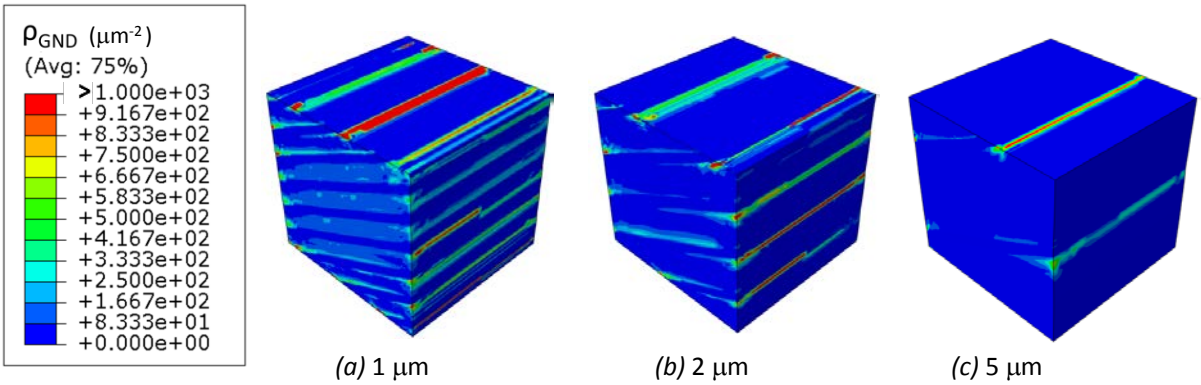

Fig.8. Contour plots of GND density for the 3 different ligament widths considered. A larger region of high GND density is predicted as α-phase ligament width is reduced from 5 μm to 1 μm due to the increased number of phase boundaries.

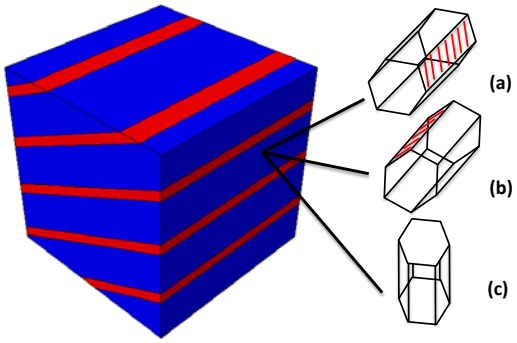

Fig. 9. The three α-phase orientations considered (a) primary slip direction near-perpendicular to β lath (b) primary slip direction near-parallel to β lath and (c) c-axis parallel to loading direction

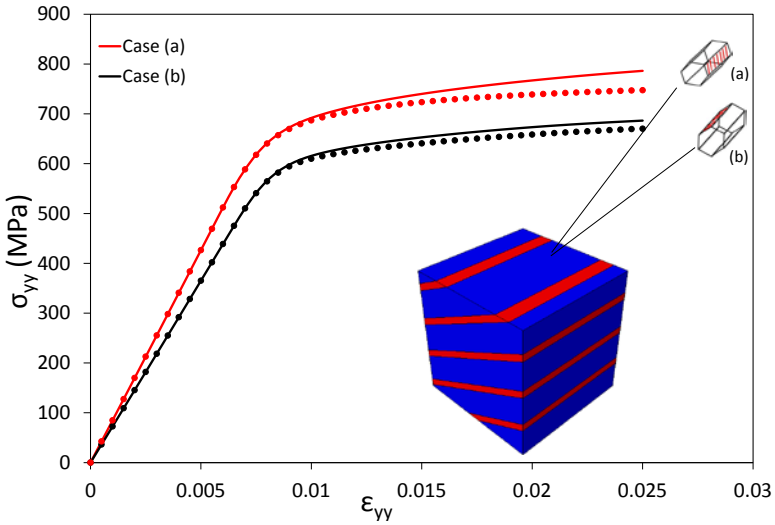

Fig. 10. Unit cell compressive stress strain response for α–phase orientation cases (a) and (b). Ligament width = 2 μm. Dotted lines represent the exclusion of length-scale effects.

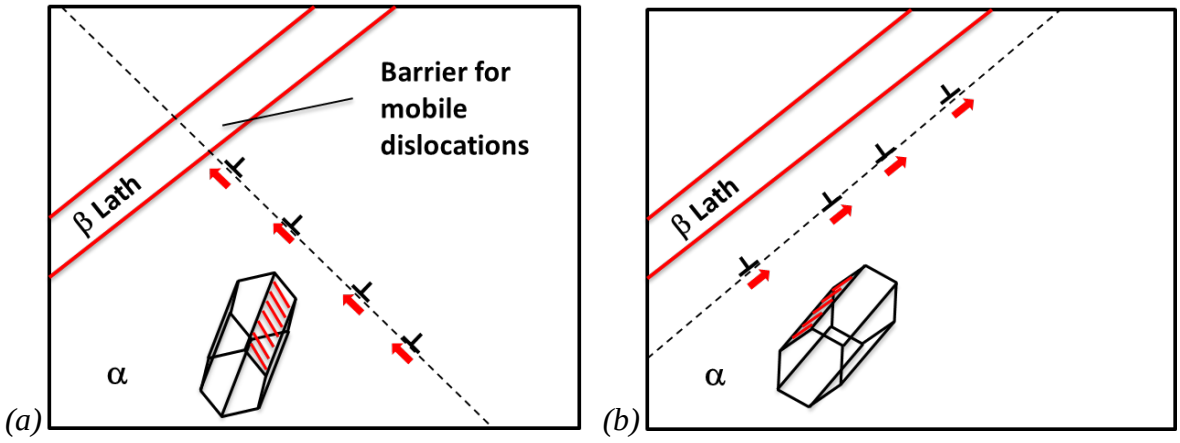

Fig.11. A schematic diagram of (a) β laths acting as barriers for mobile dislocations where the primary slip direction is aligned near-perpendicular to the laths and (b) the unrestricted flow of dislocations where the primary slip direction is aligned near-parallel to the laths.

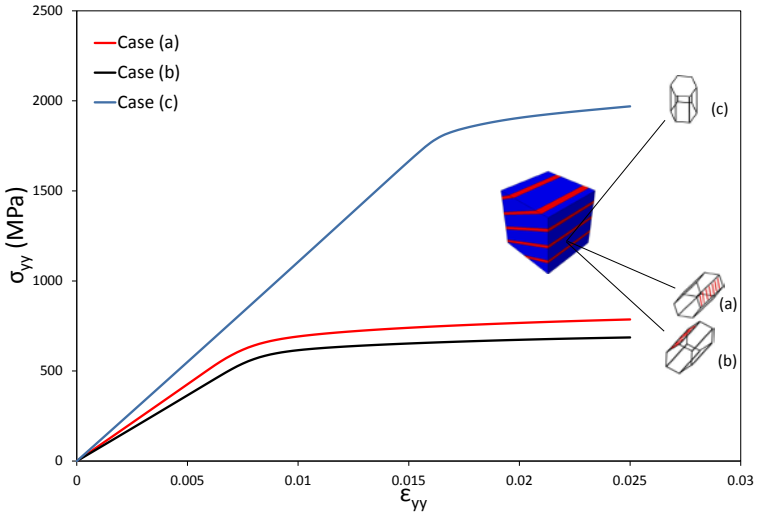

Fig.12. Unit cell compressive stress strain response for all three α–phase orientation cases. Ligament width = 2 μm.

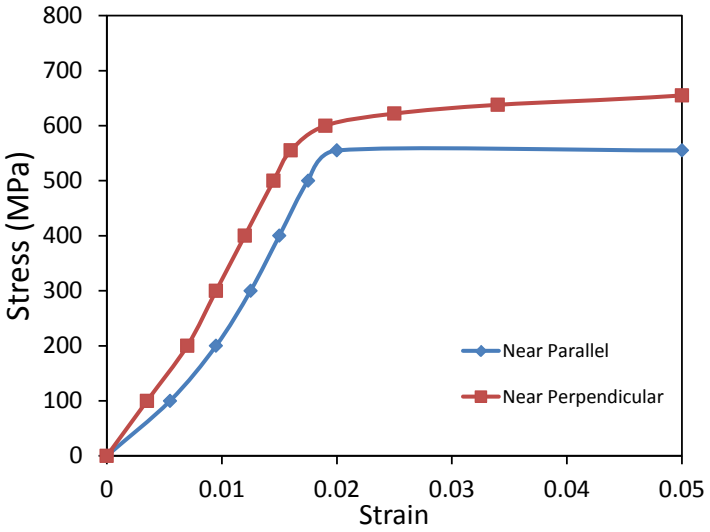

Fig.13 Experimental data adopted from Suri et al. [34].

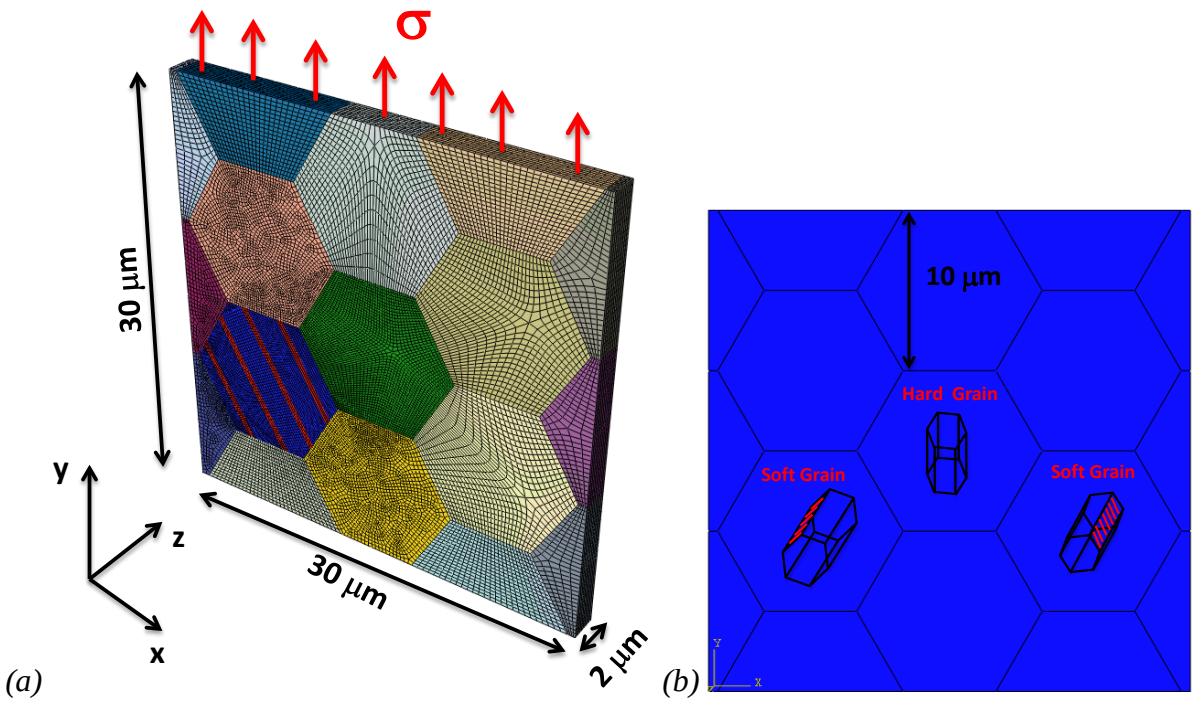

Fig. 14. Finite element model showing (a) assumed specimen geometry with element mesh and (b) the rogue grain combination. Easily activated slip systems are hatched in red.

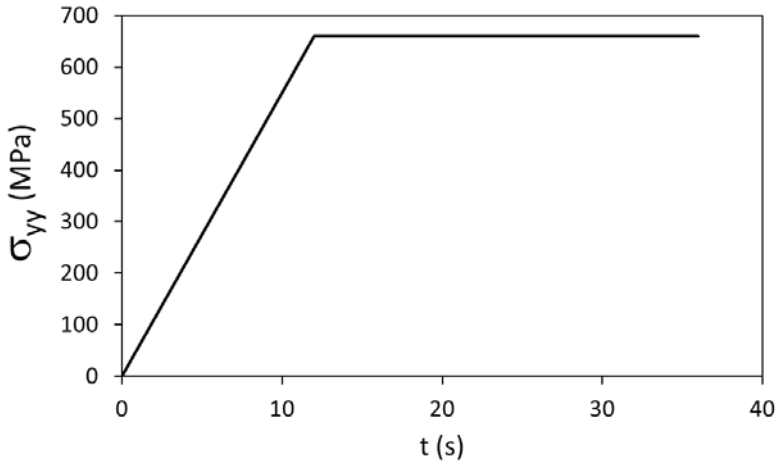

Fig. 15. Loading history showing a dwell period of 24 seconds.

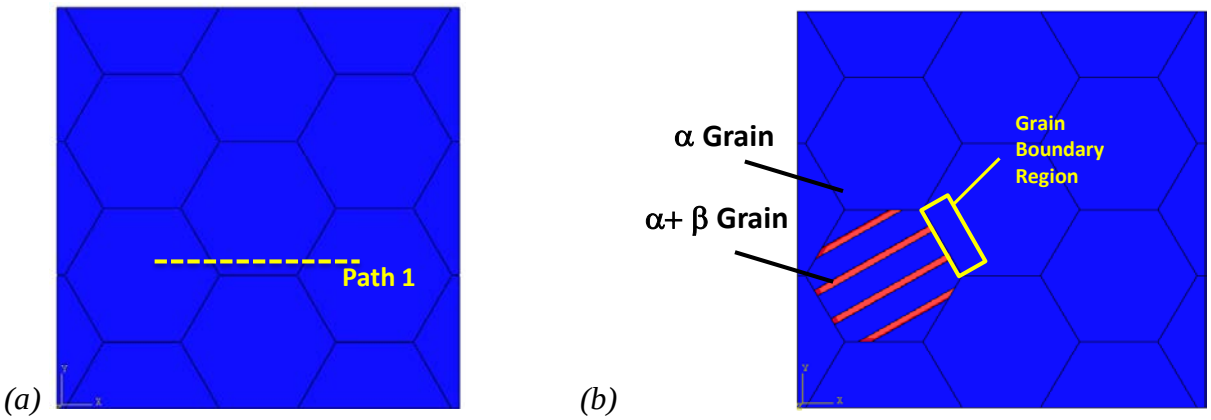

Base Case β1

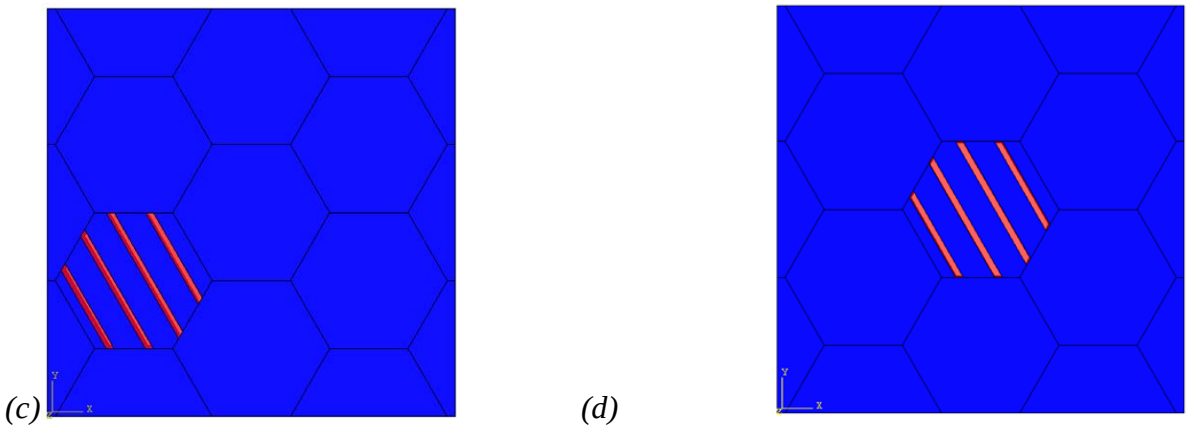

β2 β3

Fig. 16. (a) Pure α–phase base case (b) β laths near-parallel to α–phase primary slip direction in soft grain (c) β laths near-perpendicular to primary slip direction in soft grain (d) β laths in hard grain.

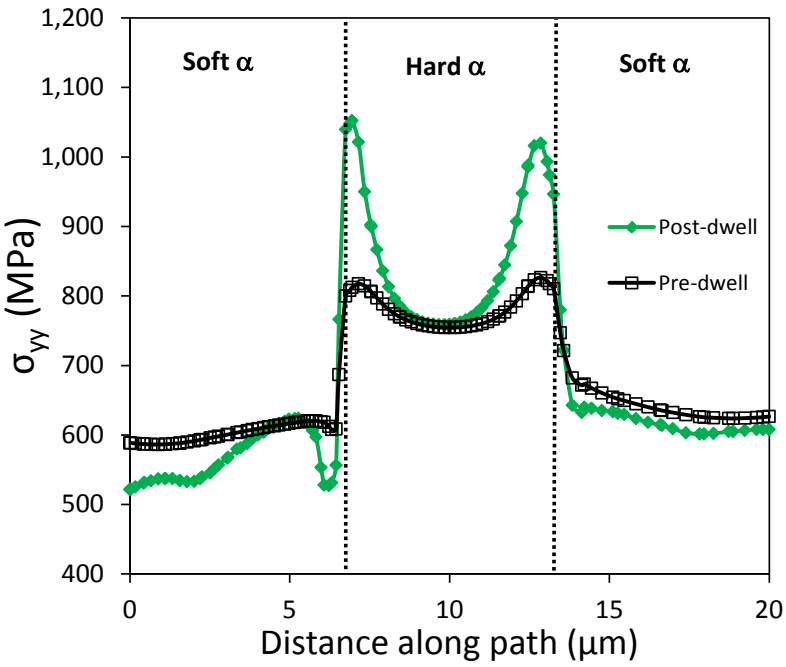

Fig. 17. Pre- and post-dwell plots of σ_{yy} along path AA for the pure α-phase base case showing significant redistribution of stress from soft grains to hard grains.

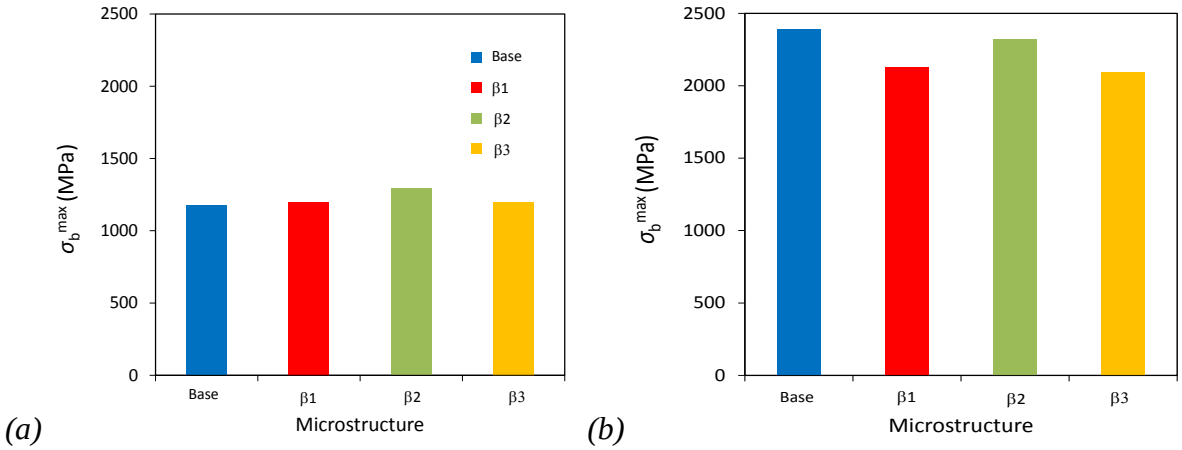

Fig. 18. Histograms showing (a) pre- and (b) post-dwell σ_b^{max} for each microstructure.

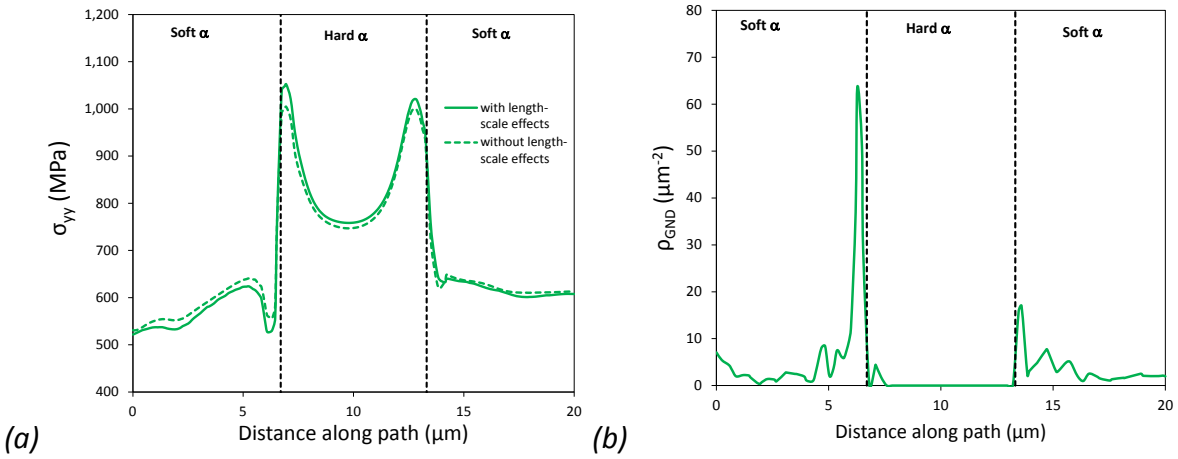

Fig. 19. Post-dwell distributions along path AA showing (a) σ_{yy} with and without length-scale effects and (b) GND density.